The process of electron acceleration during collisionless magnetic reconnection

X. R. Fu, Q. M. Lu, and S. Wang
CAS Key Laboratory of Basic Plasma Physics, School of Earth and Space Sciences, University of Science and Technology of China, Hefei, Anhui 230026, People's Republic of China

(Received 14 November 2005; accepted 15 December 2005; published online 27 January 2006)

Two-dimensional particle-in-cell simulations are performed to study electron acceleration in collisionless magnetic reconnection. The process of electron acceleration is investigated by tracing typical electron trajectories. When there is no initial guide field, the electrons can be accelerated in both the *X*-type and *O*-type regions. In the *X*-type region, the electrons can be reflected back and enter the acceleration region several times before they leave the diffusion region. In this way, the electrons can be accelerated by the inductive electric field to high energy. In the *O*-type region, the trapped electrons can be accelerated when they are trapped in the magnetic island. When there is an initial guide field, the electrons can only be accelerated in the *X*-type region, and no obvious acceleration is observed in the *O*-type region. In the *X*-type region, the electrons are not demagnetized and they gyrate with the force of the guide field. Although no electron reflection is observed in this region, the acceleration efficiency can be enhanced through staying longer time in the diffusion region due to their gyration motion. © *2006 American Institute of Physics*. [DOI: 10.1063/1.2164808]

I. INTRODUCTION

Magnetic reconnection is a fundamental plasma transport process which rapidly converts magnetic energy into plasma energy.[1–3] This conversion involves topological changes of the magnetic fields, and it also leads to both heating and acceleration of ions and electrons. Magnetic reconnection is used to explain many explosive phenomena in space and laboratory plasma, such as solar flares in the corona,[4,5] the heating of solar corona,[6,7] substorms in the Earth's magnetosphere,[8,9] and disruptions in laboratory fusion experiments.[10]

The first theoretic model for magnetic reconnection was proposed by Sweet[11] and Parker.[12] Ever since then, theoretic studies along this line have been reported in numerous articles, which include analytical theories and computer simulations. Recently the geospace environment modeling (GEM) magnetic reconnection challenge shows that the Hall term is a critical ingredient in determining the collisionless reconnection rate in the Harris current sheet model.[13] Some three-dimensional simulations are also carried out to study reconnection physics.[14–17] However, these studies focus on the reconnection rate and electromagnetic structures in magnetic reconnection. The particle dynamics, especially the electron dynamics, is paid little attention. In fact, there is observational evidence that a significant portion of the magnetic energy released during reconnection is converted into kinetic energy of energetic electrons, and the electron acceleration is one of the important signatures in magnetic reconnection. In the solar flares, x ray is thought to be generated by the energetic electrons in magnetic reconnection.[18–20] In the Earth's magnetotail, there have been direct measurements of energetic electrons during magnetic reconnection, and many consequent phenomena, such as aurora, are attributed to these energetic electrons.[21–23] Energetic electrons are also seen during sawtooth crashes and disruptions in laboratory tokamak experiments.[24]

Electron dynamics in magnetic reconnection has been previously studied using analytical theories and test particle calculations in different magnetic- and electric-field configurations.[25–28] In such studies, the electron orbits are followed in the given electromagnetic fields. The electric and magnetic fields are usually assumed to be independent of time and have a simple dependence on the spatial coordinates, while a spatially constant electric field is normally imposed along the out-of-plane direction. Therefore, direct acceleration by the reconnection electric field is the only possible mechanism for energetic electrons in these studies. Recently, several authors have investigated electron acceleration in magnetic reconnection with particle-in-cell (PIC) simulations. In PIC simulations, the particle dynamics and electromagnetic fields are solved self-consistently. Hoshino and co-workers[29,30] studied the electron acceleration process in magnetic reconnection with PIC simulations, and their model did not include the initial guide field. They found that electrons are accelerated not only around the *X*-type region due to the meandering motion but also near the magnetic-field pileup region due to the ∇B drift and the curvature drift. Ricci *et al.*[31] investigated the electron acceleration and heating for different plasma β by tracing typical electron trajectories passing through the reconnection region and found that the meandering orbits of the electrons disappear when the plasma β is decreased.

In this paper, based on a two-dimensional (2D) PIC simulation code, we explore the acceleration process of electrons in collisionless magnetic reconnection with and without the guide field by tracing typical electron trajectories. Not only the electron dynamics in the *X*-type region but also in the *O*-type region is investigated in our study. We also dis-

cuss the influence of the in-plane electric field on the electron acceleration, which has not been discussed before.

The paper is organized as follows. In Sec. II, we describe the 2D PIC simulation code. The simulation results, which focus on the acceleration process of electrons in reconnection region, are presented in Sec. III. The discussion and conclusions are given in Sec. IV.

II. SIMULATION MODEL

A 2D PIC simulation code is used in this paper to study the electron dynamics in magnetic reconnection. In the simulations, the electromagnetic fields are defined on the grids and are updated by solving the Maxwell equations with a full explicit algorithm.[32] The ions and electrons are advanced in the electromagnetic fields.

In our simulation model, the initial configuration is a one-dimensional Harris current sheet in the (x,y) plane, and the initial magnetic field can be given by[33]

$$\mathbf{B}_0(y) = B_0 \tanh\left[\left(y - \frac{L_y}{2}\right) \Big/ \delta\right]\mathbf{e}_x + B_{z0}\mathbf{e}_z, \tag{1}$$

where B_{z0} is the guide field and δ is the half-width of the current sheet. L_y is the size of the simulation domain in the y direction. The corresponding number-density is

$$n(y) = n_b + n_0 \operatorname{sech}^2\left[\left(y - \frac{L_y}{2}\right) \Big/ \delta\right], \tag{2}$$

where n_b represents a uniform, nondrift background plasma. The plasma particle distribution functions for the ions and electrons are Maxwellian, and their drift speeds in the z direction satisfy $V_{i0}/V_{e0} = -T_{i0}/T_{e0}$, where $V_{i0}(V_{e0})$ and $T_{i0}(T_{e0})$ are the drift speed and initial temperature for ions (electrons), respectively. In our simulations, the temperature ratio is $T_{i0}/T_{e0}=5$, and $n_0=5n_b$. The current sheet width is $\delta=0.5c/\omega_{\mathrm{pi}}$, where c/ω_{pi} is the ion inertial length defined using the peak Harris density n_0. The mass ratio is $m_i/m_e = 100$, and $c=20v_A$ where v_A is the Alfven speed based on B_0 and n_0.

The computation is carried out in a rectangular domain in the (x,y) plane with dimension $L_x \times L_y = (12.8c/\omega_{\mathrm{pi}}) \times (6.4c/\omega_{\mathrm{pi}})$. We employ a $N_x \times N_y = 256 \times 128$ simulation grid system, so the spatial resolution is $\Delta x = \Delta y = 0.05c/\omega_{\mathrm{pi}} = 0.5c/\omega_{\mathrm{pe}} = 3\lambda_{\mathrm{De}}$, where λ_{De} is the electron Debye length. The time step is $\omega_{\mathrm{pe}}\Delta t = 0.3$ or equivalently $\Omega_i \Delta t = 0.0015$. In all runs we employ more than 1.0×10^6 particles per species to represent the plasma of the Harris current sheet, and the same number of particles is used to represent the background plasma. The periodic boundary conditions are used along the x direction. The ideal conducting boundary conditions for electromagnetic fields are employed in the y direction, and particles are reflected after they reach the boundaries.

In order to put the system in the nonlinear regime from the beginning of the simulation, an initial flux perturbation is introduced to modify the Harris current sheet configuration, which has the form

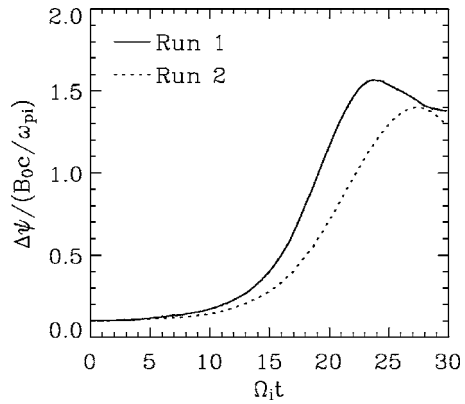

FIG. 1. Time history of the reconnection magnetic flux for run 1 (solid line) and run 2 (dash line).

$$\psi(x,y) = \psi_0 \cos\left[2\pi\left(x - \frac{L_x}{2}\right) \Big/ L_x\right] \cos\left[\pi\left(y - \frac{L_y}{2}\right) \Big/ L_y\right], \tag{3}$$

where ψ is the vector potential component A_z, and the value of ψ_0 is chosen as $\psi_0/(B_0c/\omega_{\mathrm{pi}}) = 0.05$.

III. SIMULATION RESULTS

In this paper, we perform 2D PIC simulations to investigate the effect of in-plane and out-of-plane electric fields on electron acceleration. Two cases are run in the simulations, runs 1 and 2, whose initial guide fields are $B_{z0}/B_0 = 0$ and $B_{z0}/B_0 = 1$, respectively.

A. The electric fields in the diffusion region

Previous particle and hybrid simulations have shown that the nonlinear reconnection rate will be substantially modified when the guide field is sufficiently large. Figure 1 shows the time evolution of the reconnected magnetic flux $\Delta\psi$ for runs 1 and 2. Here the magnetic flux $\Delta\psi$ is defined as the flux difference between the X and O lines, and its slope can be served as an indicator of the magnetic reconnection rate. Similar to previous simulations, the reconnection rate in run 2 is substantially smaller than that in run 1. In run 1, the magnetic flux $\Delta\psi$ begins to increase at $\Omega_i t \sim 10$ and reaches its maximum value of $\Delta\psi/(B_0c/\omega_{\mathrm{pi}}) \sim 1.6$ at $\Omega_i t \sim 23$. In run 2, the magnetic flux $\Delta\psi$ begins to increase at $\Omega_i t \sim 10$ and reaches its maximum value of $\Delta\psi/(B_0c/\omega_{\mathrm{pi}}) \sim 1.4$ at $\Omega_i t \sim 27$. From the figure, we can also find that the fastest reconnection rate occurs at $\Omega_i t \sim 19$ and $\Omega_i t \sim 23$ for runs 1 and 2, respectively.

Figure 2 shows contours of (a) the electric field in the x direction $(c/v_A)E_x/B_0$, (b) the electric field in the y direction $(c/v_A)E_y/B_0$, (c) the out-of-plane electric field $(c/v_A)E_z/B_0$, and (d) the out-of-plane magnetic field B_z/B_0 averaged over the time interval $18.9 < \Omega_i t < 19.1$ when the reconnection rate attains its maximum during its time evolution for run 1. The magnetic-field lines at $\Omega_i t = 19$ are also presented in the figure. The maximum island width is about $1.0c/\omega_{\mathrm{pi}}$. Due to the in-plane Hall currents the out-of-plane magnetic-field

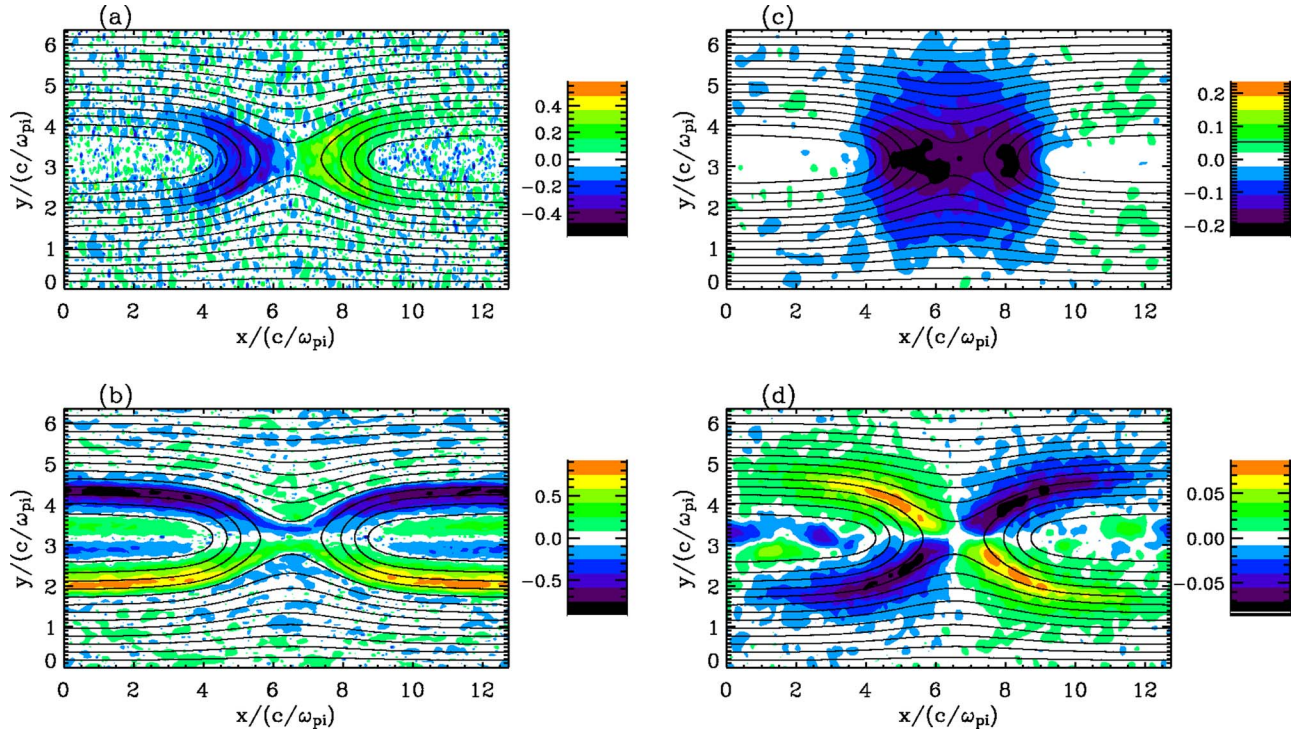

FIG. 2. (Color online) Contours of (a) the electric field in the x direction $(c/\nu_A)E_x/B_0$, (b) the electric field in the y direction $(c/\nu_A)E_y/B_0$, (c) the out-of-plane electric field $(c/\nu_A)E_z/B_0$, and (d) the out-of-plane magnetic field B_z/B_0 averaged over the time interval $18.9<\Omega_i t<19.1$ for run 1. The magnetic-field lines at $\Omega_i t=19$ are also presented.

component B_z exhibits the characteristic quadrupole pattern with the maximum amplitude of about $0.1B_0$. E_x forms a bicrescent shape symmetric along $x=L_x/2$ with a negative value in region $x<L_x/2$ and a positive value in region $x>L_x/2$, while E_y forms two strips symmetric along $y=L_y/2$ with a positive value in region $y<L_y/2$ and a negative value in region $y>L_y/2$. The inductive electric field E_z is roughly circular with the center at the X line and a radius about $3.0c/\omega_{\mathrm{pi}}$. Similar electromagnetic structure has also been obtained by Pritchett[32] and Hoshino.[30]

Figure 3 shows contours of (a) the electric field in the x direction $(c/\nu_A)E_x/B_0$, (b) the electric field in the y direction $(c/\nu_A)E_y/B_0$, (c) the out-of-plane electric field $(c/\nu_A)E_z/B_0$, and (d) the fluctuating out-of-plane magnetic field $B_z'=(B_z-B_{z0})/B_0$ averaged over the time interval $22.9<\Omega_i t<23.1$ when the reconnection rate attains its maximum during its time evolution for run 2. The magnetic-field lines at $\Omega_i t=23$ are also presented in the figure. Compared with the case with initial guide field $B_{z0}/B_0=0$, there is no obvious difference for the shape of the magnetic-field lines in the x-y plane and the inductive electric field E_z in the diffusion region, and now E_z has smaller value due to the reduced reconnection ratio. However, the quadrupole pattern of the fluctuating field B_z' is distorted, and the positive value occupies most of the region inside the magnetic island while the negative value occupies a small region exterior to the magnetic island. The symmetry of E_x and E_y is also destroyed. The regions above and below the X line are occupied by the electric field in the $+x$ and $-x$ directions, respectively. Pritchett and Coroniti also obtained similar structure with three-dimensional (3D) PIC simulations.[15]

B. Electron dynamics during magnetic reconnection

We investigate the process of electron acceleration during collisionless magnetic reconnection by tracing several typical electron trajectories. Figure 4 depicts two typical electron trajectories for run 1. The first electron passes through the X-type region during the time period from $\Omega_i t=18.5$ to $\Omega_i t=20$, and its start and end points are denoted by A1 and E1. The second electron is trapped in the O-type region during the time period from $\Omega_i t=17.5$ to $\Omega_i t=19.5$, and its start and end points are denoted by A2 and D2. The time evolutions of (a) the kinetic energy, (b) ν_x/ν_A, (c) ν_y/ν_A, and (d) ν_z/ν_A of the first electron for run 1 are presented in Fig. 5. The electron starts at A1, and from B1 the electron begins to enter the X-type region, where it is demagnetized. The period from B1 to C1 describes the electron dynamics in the X-type region, where the electron is reflected by the electric field E_y twice and is trapped in the X-type region. During this period the electron obtains high energy because it is accelerated by the reconnection electric field E_z and gets large positive ν_z. After the electron arrives at C1, it enters the magnetic-field line pileup region. With the force of the magnetic field and the electric field E_x, the electron dynamics is complicated. The electron is accelerated by the inductive electric field E_z when it has positive ν_z, and it is decelerated by E_z when it have negative E_z. However, in average, there is no obvious increase of the electron kinetic energy during the period from C1 to D1 in the magnetic-field line pileup region. At the position D1, the electron obtains a positive velocity in the y direction ν_y and begins to enter the lobe region. During the period from D1 to E1, the electron velocity

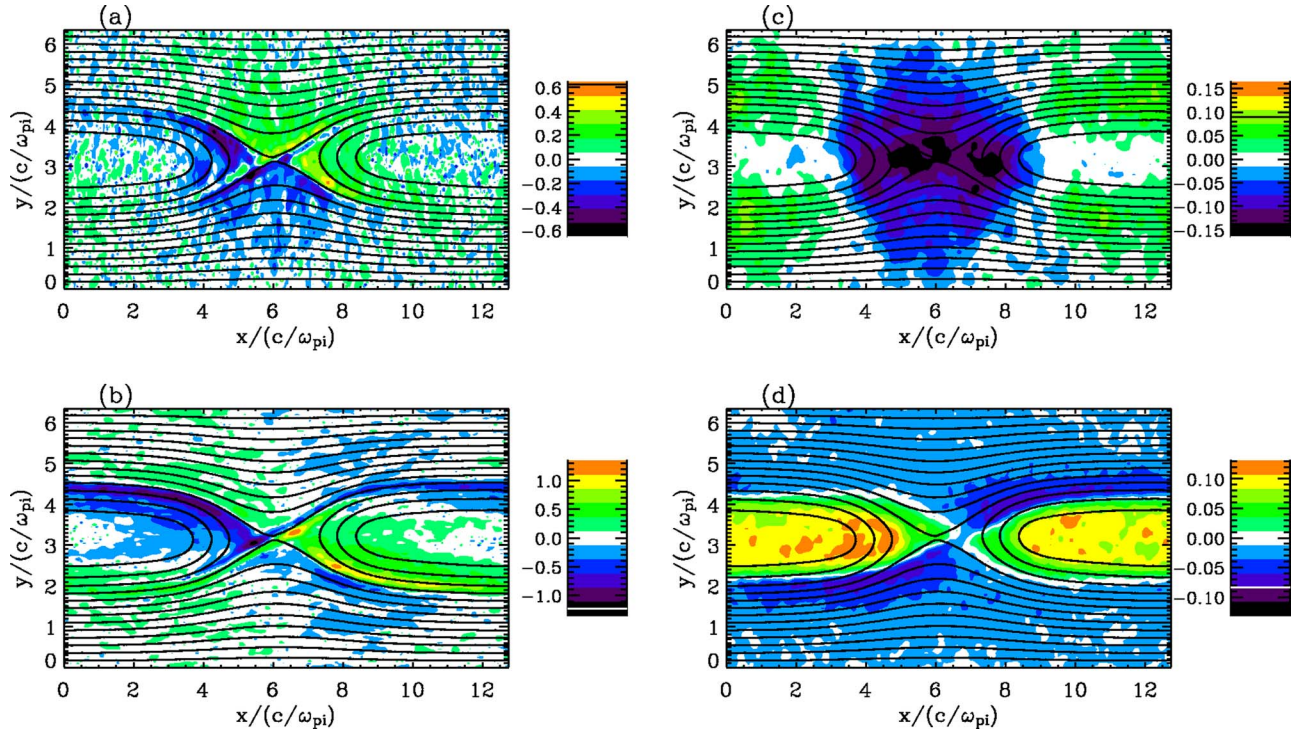

FIG. 3. (Color online) Contours of (a) the electric field in the x direction $(c/v_A)E_x/B_0$, (b) the electric field in the y direction $(c/v_A)E_y/B_0$, (c) the out-of-plane electric field $(c/v_A)E_z/B_0$, and (d) the fluctuating out-of-plane magnetic field $B_z'=(B_z-B_{z0}$ averaged over the time interval $22.9<\Omega_i t<23.1$ for run 2. The magnetic-field lines $\Omega_i t=23$ are also presented.

is diverted to the $-x$ direction and gains an outflow velocity along the magnetic field. Figure 6 shows the time evolutions of the velocities (a) the kinetic energy, (b) v_x/v_A, (c) v_y/v_A, and (d) v_z/v_A of the second electron for run 2. Note that in our simulations periodical boundary condition is used in the x direction, and particles leaving one side will enter the simulation domain from the other side. From position A2, the electron moves to the $+x$ direction and it is reflected at position B2, where the electron attains larger absolute value of v_x. At the same time, the electron is also accelerated in the $+z$ direction by E_z. At the position C2, the electron is reflected again and accelerated with the same mechanism. In this way, the electron obtains high energy gradually. It should be mentioned that in this region the motion of the electron is nonadiabatic because its gyroradius is comparable with the radius of curvature of the magnetic-field lines,[34,35] and the electron is only accelerated before the quasiequilibrium stage is reached. Therefore, the electron can be stochastically accelerated when it is trapped in the magnetic island, and the process is also related to the evolution of the magnetic island.

Figure 7 depicts two typical electron trajectories for run

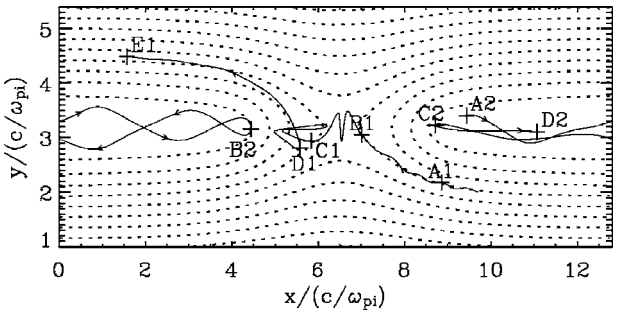

FIG. 4. Two typical electron trajectories in (x,y) for run 1. The first electron passes through the X-type region during the time period from $\Omega_i t=18.5$ to $\Omega_i t=20$, and its start and end points are denoted by A1 and E1. The second electron is trapped in the O-type region during the time period from $\Omega_i t=17.5$ to $\Omega_i t=19.5$, and its start and end points are denoted by A2 and D2. The dash lines in the figure show the magnetic-field lines at $\Omega_i t=18.5$.

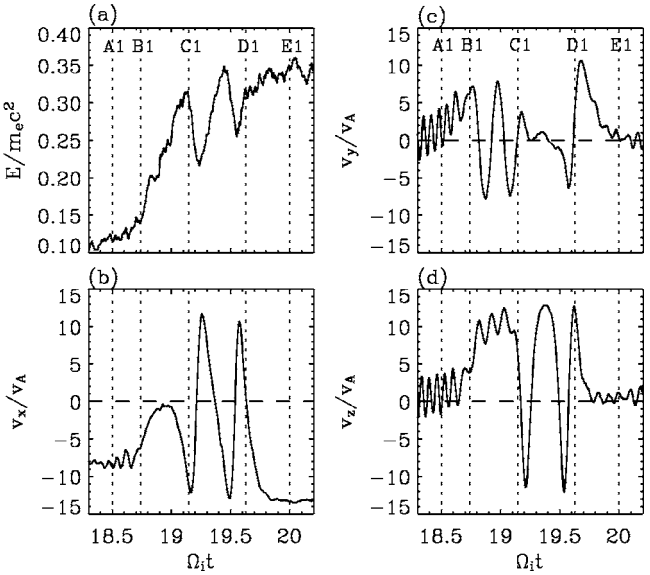

FIG. 5. The time evolution of (a) the kinetic energy, (b) v_x/v_A, (c) v_y/v_A, and (d) v_z/v_A, of the first electron for run 1. The key position corresponding to Fig. 4 is marked by vertical dash lines.

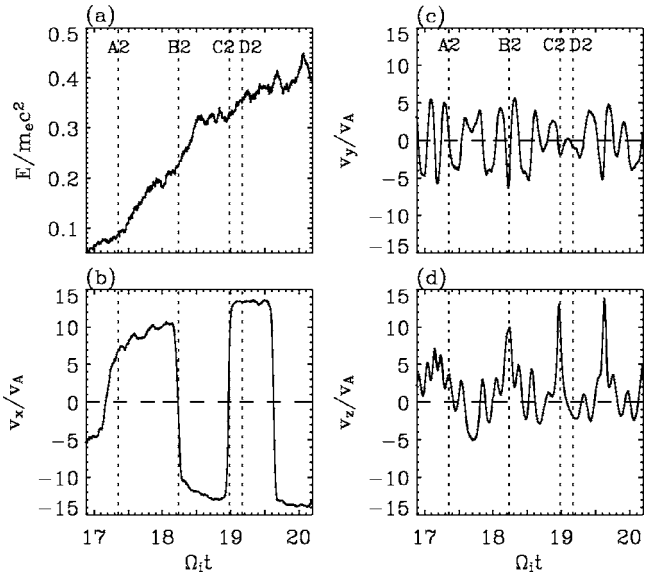

FIG. 6. The time evolution of (a) the kinetic energy, (b) v_x/v_A, (c) v_y/v_A, and (d) v_z/v_A, of the second electron for run 1. The key position corresponding to Fig. 4 is marked by vertical dash lines.

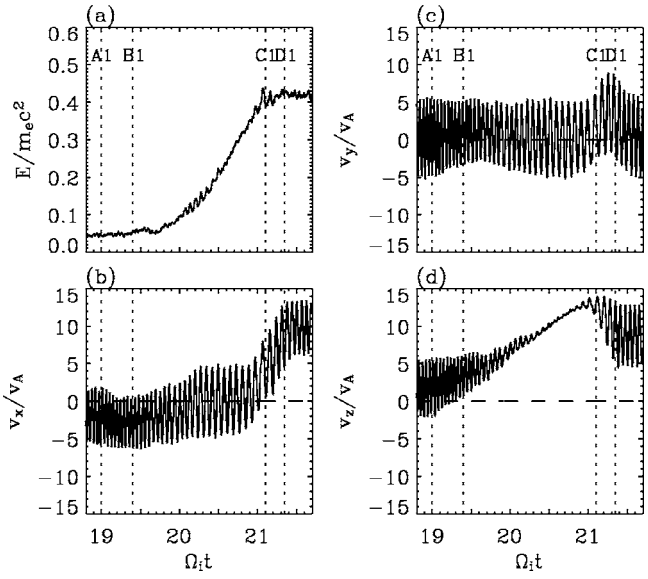

FIG. 8. The time evolution of (a) the kinetic energy, (b) v_x/v_A, (c) v_y/v_A, and (d) v_z/v_A, of the first electron for run 2. The key position corresponding to Fig. 4 is marked by vertical dash lines.

2. The first electron passes through the *X*-type region during the time period from $\Omega_i t=19$ to $\Omega_i t=21.5$, and its start and end points are denoted by A1 and D1. The second electron is trapped in the *O*-type region during the time period from $\Omega_i t=17.5$ to $\Omega_i t=21$, and its start and end points are denoted by A2 and D2. The time evolutions of (a) the kinetic energy, (b) v_x/v_A, (c) v_y/v_A, and (d) v_z/v_A, of the first electron for run 2 are presented in Fig. 8. The position of the electron starts at A1, which is in the lobe region. When the electron is in the *X*-type region from B1 to C1, it is accelerated by the inductive electric field E_z. Now in the diffusion region the electron is not demagnetized due to the existence of the magnetic field B_z, and it gyrates in the diffusion region. No reflection by the magnetic or electric forces is observed when the electron is in the diffusion region. In general the electrons stay in the diffusion region for longer time than run 1 due to their gyration, and they can be accelerated to higher energy by the inductive electric field E_z. After the electron leaves the *X*-type region at position C1, it is diverted by the magnetic field to the $+x$ direction and leaves the *X*-type region along the magnetic field. The second electron is trapped in the *O*-type region, and the time evolutions of its velocities (a) the kinetic energy, (b) v_x/v_A, (c) v_y/v_A, and (d) v_z/v_A are presented in Fig. 9. Because the motion of the electron is mainly controlled by the magnetic field B_z, it gyrates in the *O*-type region and its motion is adiabatic. Although the electron is reflected at position B2 and C2, no obvious acceleration is observed.

Figure 10 shows the electron energy spectrum integrated over the pitch angle for (a) run 1 and (b) run 2. Electron acceleration can be obviously found in the figure. The high-energy parts of the electron distributions approximately fit a

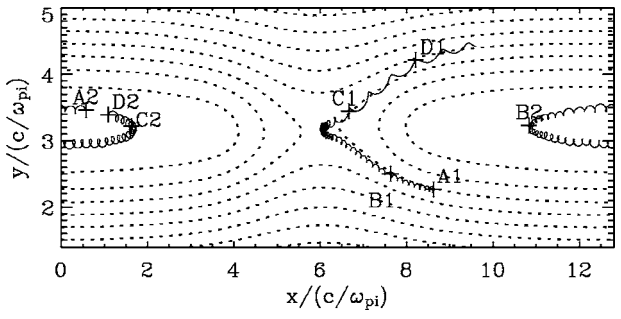

FIG. 7. Two typical electron trajectories in (x,y) for run 2. The first electron passes through the *X*-type region during the time period from $\Omega_i t=19$ to $\Omega_i t=21.5$, and its start and end points are denoted by A1 and D1. The second electron is trapped in the *O*-type region during the time period from $\Omega_i t=17.5$ to $\Omega_i t=19$, and its start and end points are denoted by A2 and D2. The dash lines in the figure show the magnetic-field lines at $\Omega_i t=19.5$.

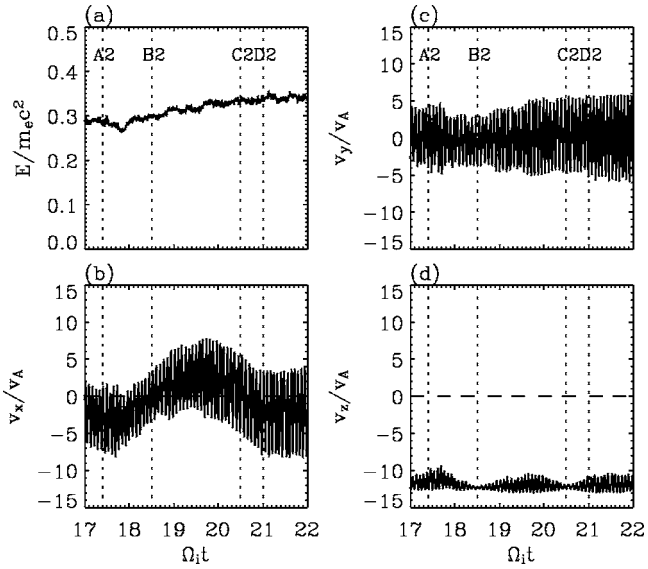

FIG. 9. The time evolution of (a) the kinetic energy, (b) v_x/v_A, (c) v_y/v_A, and (d) v_z/v_A of the second electron for run 2. The key position corresponding to Fig. 4 is marked by vertical dash lines.

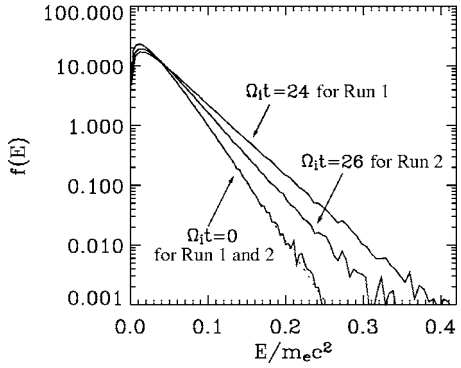

FIG. 10. The electron energy spectrum integrated over the pitch angle for runs 1 and 2. The spectrum is obtained at $\Omega_i t=24$ for run 1 and $\Omega_i t=26$ for run 2. The electron energy spectrum at initial time is also presented in the figure.

power law distribution, $f \propto E^{-\alpha}$, where the power indices α are about 5.8 and 6.2 for runs 1 and 2, respectively. There are more high-energy electrons in run 1, because in run 2 the electrons are only accelerated in the *X*-type region while in run 1 the electrons can be accelerated both in *X*-type and *O*-type regions. This point can be demonstrated in Fig. 11, which shows the positions of the energetic electrons whose energy is larger than $0.3mc^2$ for (a) run 1 and (b) run 2. In run 2, the energetic electrons are concentrated in the lobe, where the electrons have just left from the diffusion region after they are accelerated. In run 1, the energetic electrons are also found in the magnetic island.

IV. CONCLUSIONS AND DISCUSSIONS

Energetic electrons are an important signature of magnetic reconnection. In this paper, with 2D PIC simulations, we investigate the process of electron acceleration in both the *X*-type and *O*-type regions during magnetic reconnection with and without the guide field by tracing the typical electron trajectories. During the magnetic reconnection without the initial guide field B_z, the electrons can be accelerated in both the *X*-type and *O*-type regions. In the *X*-type region, after the electrons enter the diffusion region, they can be reflected by the combination of magnetic and electric forces and reenter the region several times. Therefore, the electrons can be accelerated several times in the diffusion region by the inductive electric field E_z to high energy. In the *O*-type region, the motions of the trapped electrons are stochastic, and they can be accelerated when they are reflected by the magnetic island. The process of electron acceleration is also related to the evolution of the magnetic island. During magnetic reconnection with the initial guide field $B_z/B_0=1$, the electrons can only be accelerated in the *X*-type region. In the *X*-type region, the electrons are no longer demagnetized and they gyrate with the force of the magnetic field B_z. The electrons are diverted to the x direction and leave the diffusion region directly after they are accelerated in the z direction by the inductive electric field. No electron reflection is observed in this region. However, due to their gyration motion, the electrons can stay for a longer time and the acceleration efficiency is enhanced. In general, there are more energetic electrons in the diffusion region during magnetic reconnection with the initial guide field. The power index of the electron energy spectrum is larger in the magnetic reconnection with the initial guide field than that without the initial guide field, because the electrons can be accelerated in both the *X*-type and *O*-type regions during magnetic reconnection without the initial guide field.

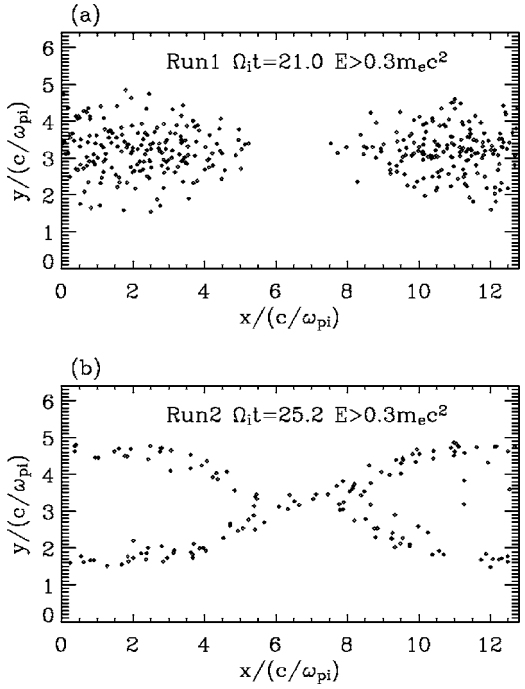

FIG. 11. The positions of the energetic electrons whose energy is larger than $0.3mc^2$ for (a) run 1 and (b) run 2.

The process of electron acceleration during magnetic reconnection has also been conducted by Ricci *et al.*[31] and Hoshino and co-workers,[29,30] where they focused the electron acceleration in the *X*-type region. Ricci *et al.*[31] used an implicit PIC code with coarse grid size and time step, which cannot resolve the details of the process of electron acceleration discussed in the paper. Hoshino and co-workers[29,30] found that the electrons can be accelerated in the magnetic-field pileup region as well as in the diffusion region. However, our study shows that there is no further electron acceleration in the pileup region, and it is consistent with the Wind spacecraft observations.[23] In this paper we use unrealistic ion-to-electron mass ratio and light speed. Mass ratio is considered to have a strong influence on the electron acceleration, and we think that the energetic electrons can be accelerated to much more higher energy if a realistic ion-to-electron mass ratio is used. Although the mechanisms of electron acceleration during magnetic reconnection can be well understood from our study, it is difficult to compare the electron energy with the observations at present.

ACKNOWLEDGMENTS

This research was supported by the National Science Foundation of China (NSFC) under Grant Nos. 40336052, 40304012, and 40404012 and by the Chinese Academy of Sciences Grant No. KZCX3-SW-144.

[1]D. Biskamp, *Magnetic Reconnection in Plasmas* (Cambridge University Press, Cambridge, 2000).
[2]E. R. Priest and T. Forbes, *Magnetic Reconnection: MHD Theory and Applications* (Cambridge University Press, New York, 2000).
[3]V. M. Vasyliunas, Rev. Geophys. **13**, 303 (1975).
[4]R. G. Giovanelli, Nature (London) **158**, 81 (1946).
[5]S. Tsuneta, H. Hara, T. Shimizu, L. W. Acton, K. T. Strong, H. S. Hudson, and Y. Ogawara, Publ. Astron. Soc. Jpn. **44**, L63 (1992).
[6]P. Ulmschneider, E. R. Priest, and R. Rosner, in *Mechanisms of Chromospheric and Coronal Heating*, edited by R. Rosner (Springer-Verlag, Berlin, 1991).
[7]P. A. Cargill and J. A. Klimchuk, Astrophys. J. **478**, 799 (1997).
[8]A. Nishida, *Geomagnetic Diagnostics of the Magnetosphere* (Springer-Verlag, New York, 1978).
[9]W. J. Hughes, in *Introduction to Space Physics*, edited by M. G. Kivelson and C. T. Russell (Cambridge University Press, New York, 1995), p. 227.
[10]J. Wesson, *Tokomaks* (Oxford University Press, New York, 1997).
[11]P. A. Sweet, in *Electromagnetic Phenomena in Cosmical Physics*, edited by B. Lehnert (Cambridge University Press, New York, 1958), p. 123.
[12]E. N. Parker, J. Geophys. Res. **62**, 509 (1957).
[13]J. Birn, J. F. Drake, M. A. Shay *et al.*, J. Geophys. Res. **106**, 3715 (2001).
[14]M. Hesse and M. Kuznetsova, J. Geophys. Res. **106**, 29831 (2001).
[15]P. L. Pritchett and F. V. Coroniti, J. Geophys. Res. **109**, A01220 (2004).
[16]A. Zeiler, D. Biskamp, J. F. Drake, B. N. Rogers, M. A. Shay, and M. Scholer, J. Geophys. Res. **107**, 1230 (2002).
[17]M. Scholer, I. Sidorenko, C. H. Jaroschek, R. A. Treumann, and A. Zeiler, Phys. Plasmas **10**, 3521 (2003).
[18]R. P. Lin and H. S. Hudson, Sol. Phys. **17**, 412 (1971).
[19]R. P. Lin and H. S. Hudson, Sol. Phys. **50**, 153 (1976).
[20]J. A. Miller, P. J. Cargill, A. Emslie, G. D. Holamn, B. R. Dennis, T. N. Larosa, R. M. Winglee, S. G. Benka, and S. Tsuneta, J. Geophys. Res. **102**, 14631 (1997).
[21]D. N. Baker and E. C. Stone, Geophys. Res. Lett. **3**, 557 (1976).
[22]D. N. Baker and E. C. Stone, J. Geophys. Res. **82**, 1532 (1977).
[23]M. Øieroset, R. P. Lin, T. D. Phan, D. E. Larson, and S. D. Bale, Phys. Rev. Lett. **89**, 195001 (2002).
[24]P. V. Savrukhin, Phys. Rev. Lett. **86**, 3036 (2001).
[25]Y. E. Litvinenko, Astrophys. J. **462**, 997 (1996).
[26]H. J. Deeg, J. Borovsky, and N. Duric, Phys. Fluids B **3**, 2660 (1991).
[27]P. K. Browning and G. E. Vekstein, J. Geophys. Res. **106**, 18677 (2001).
[28]P. Wood and T. Neukirch, Sol. Phys. **226**, 73 (2005).
[29]M. Hoshino, T. Mukai, T. Terasawa, and I. Shinohara, J. Geophys. Res. **106**, 25979 (2001).
[30]M. Hoshino, J. Geophys. Res. **110**, A10215 (2005).
[31]P. Ricci, G. Lapenta, and J. U. Brackbill, Phys. Plasmas **10**, 3554 (2003).
[32]P. L. Prichett, J. Geophys. Res. **106**, 3783 (2001).
[33]E. G. Harris,Nuovo Cimento **23**, 115 (1962).
[34]J. Chen and P. J. Palmadesso, J. Geophys. Res. **91**, 1499 (1986).
[35]R. Smets, D. Delcourt, and D. Fontaine, J. Geophys. Res. **103**, 20407 (1998).